



Published in final edited form as:

Ann Biomed Eng. 2011 February ; 39(2): 714–729. doi:10.1007/s10439-010-0192-2.

Initial Fiber Alignment Pattern Alters Extracellular Matrix Synthesis in Fibroblast Populated Fibrin Gel Cruciforms and Correlates with Predicted Tension

E.A. Sander¹, V.H. Barocas¹, and R.T. Tranquillo^{1,2,*}

¹Department of Biomedical Engineering, University of Minnesota, Minneapolis, MN 55455

²Department of Chemical Engineering & Materials Science, University of Minnesota, Minneapolis, MN 55455

Abstract

Human dermal fibroblasts entrapped in fibrin gels cast in cross-shaped (cruciform) geometries with 1:1 and 1:0.5 ratios of arm widths were studied to assess whether tension and alignment of the cells and fibrils affected ECM deposition. The cruciforms of contrasting geometry (symmetric vs. asymmetric), which developed different fiber alignment patterns, were harvested at 2, 5, and 10 weeks of culture. Cruciforms were subjected to planar biaxial testing, polarimetric imaging, DNA and biochemical analyses, histological staining, and SEM imaging. As the cruciforms compacted and developed fiber alignment, fibrin was degraded and elastin and collagen were produced in a geometry-dependent manner. Using a continuum mechanical model that accounts for direction-dependent stress due to cell traction forces and cell contact guidance with aligned fibers that occurs in the cruciforms, the mechanical stress environment was concluded to influence collagen deposition, with deposition being greatest in the narrow arms of the asymmetric cruciform where stress was predicted to be largest.

Keywords

Fibrin; Collagen; Remodeling; Mechanical Properties; Tension

INTRODUCTION

Engineered tissues are necessary to replace diseased and damaged tissues incapable of healing on their own. For engineered tissues to be functional, they must possess mechanical properties similar to the native tissues they are intended to replace [1]. These properties derive from the heterogeneous composition and anisotropic organization of the tissue's microstructure [2]. For many tissues, including skin, ligaments, and arteries, the most important load-bearing component of the tissue is collagen [3]. However, it is the arrangement or alignment pattern of the collagen fibrils rather than the mere presence of collagen that controls the tissue's mechanical functionality. Consequently, to produce a mechanically functional replacement tissue requires at least some recapitulation of the tissue's organization in the engineered construct as well as its composition.

One method employed to produce engineered tissues with a prescribed fiber alignment pattern involves cell entrapment in a collagen or fibrin gel constrained by specially designed

*to whom all correspondence should be addressed, 7-114 NHH, 312 Church St. SE, Minneapolis, MN 55455, tranquillo@cems.umn.edu, phone: (612) 626-6868, fax: (612) 626-6583.

molds [4 – 7]. This strategy of cell-induced fiber alignment has been used to produce a number of engineered tissues, including blood vessels [5,8], heart valve leaflets [6,7], and tendons [9,10]. As the cells compact the gel, the combination of cell traction forces, gel geometry, and mechanical constraints exerted by the mold on the compacting gel results in aligned fibers [11] that both mimic fiber alignment patterns found in native tissue and improve the mechanical properties of the construct.

When cells are entrapped in a fibrin gel instead of a collagen gel, the initial fibrin fiber alignment pattern that arises during the early stages of compaction serves as a template that is gradually degraded and replaced with organized collagen and other extracellular matrix (ECM) proteins [8]. In addition, fibrin-based constructs demonstrate greater collagen synthesis and better mechanical properties after remodeling than their collagen-based counterparts [8]. However, there remains much to understand in terms of how the tissue's microstructure and mechanical behavior evolves during the remodeling response, and how this process can be better controlled to produce a functional replacement tissue.

Biochemical stimulation with chemical factors like TGF- β , ascorbic acid, and insulin [8,12–15] provides some control over matrix synthesis and can increase the strength and modulus of fibrin-based tissue constructs, as does mechanical stimulation with statically and dynamically applied loads [16]. Similar stimulatory effects from loading have been shown in other systems [17–19].

Another potentially significant factor in the remodeling outcome is the endogenous cell tension that develops during the compaction process. Several studies have shown that cell tension provides an important stimulatory signal that is reduced or absent in unconstrained, free-floating gels [19–21]. In our system, through the interplay of cell-induced gel compaction, gel geometry, and mold constraints on gel compaction, an initially homogeneous and isotropic fibroblast-populated fibrin gel is transformed into a heterogeneous and anisotropic tissue construct with an organized fiber alignment pattern [11,22]. Fiber alignment in turn induces cell alignment via contact guidance [23], thus creating a complex and dynamic distribution of mechanical stresses in the construct driven by cell traction forces. The regional differences in the local mechanical environment may in turn direct the ultimate pattern of fibrin remodeling into tissue.

In a previous study, we examined the relationship between mechanical anisotropy and fiber alignment on cell-compacted, cross-shaped collagen gels (cruciforms) [22]. The cruciform geometry provides a biaxially loaded specimen that more closely approximates the multiaxial loading environment experienced by most tissues. More importantly, it allows one to control the fiber alignment pattern, and hence mechanical anisotropy of the construct, by varying the aspect ratio of the cruciform arm widths. To understand better the role of fiber alignment in the remodeling process, we used this well-controlled cruciform test system [22,24,25] to determine whether differences in the induced fibrin fiber alignment pattern results in differences in the remodeling process, such as the amount of collagen produced, and whether such differences translate into altered mechanical properties.

MATERIALS AND METHODS

Cell Culture

Neonatal human dermal fibroblasts (nHDFs) (Clonetics) were cultured in a 50:50 mix of Dulbecco's modified Eagles medium and Hams F12 medium (DMEM/F12) (Gibco) with 10% fetal bovine serum (FBS) (Hyclone Laboratories), 100 units/mL penicillin (Gibco), 100 μ g/mL streptomycin, and 2.5 μ g/mL amphotericin-B. Cells were passaged at 100% confluency and harvested from passages 9 and 10.

Cross-Shaped Teflon Molds

The fiber alignment pattern that develops in the cell-compacted gels can be controlled by altering the aspect ratio of the channel widths (arms) in cross-shaped Teflon molds (cruciforms) [22,24,25]. At one limit, when the arm widths are symmetric, an equibiaxially loaded isotropic region develops in the cruciform center. By reducing the arm width of one axis while maintaining the width of the other, the effect of increasing alignment in the center can be examined. In this experiment, two mold geometries with differing channel widths were examined: a symmetric 1:1 aspect ratio, in which all four cruciform arms are 8 mm wide, and an asymmetric 1:0.5 aspect ratio, in which the vertical axis (4 mm) is half the width of the horizontal axis (8 mm) (Fig. 1A). These geometries were selected in order to compare the remodeling response occurring in isotropic versus aligned gels and their corresponding isotropic and anisotropic stress states. Cruciform dimensions were chosen so that the cruciforms would fit in a 6-well tissue culture plate, produce a sample large enough to conduct biaxial mechanical testing, and accommodate the aspect ratios used in this study. To enable mechanical testing of compacted cruciforms directly from the mold, our previous mold was modified to allow the gel to compact around 2-mm diameter borosilicate rods spanning each channel at the distal end of each arm (Fig. 1B). The rods passed through the centers of Teflon pins positioned on each side of the channel. For each geometry and time point, seven constructs were made: three for mechanical testing and biochemical analysis, three for cell number, and one for histology (plus two extra for a total of 44 constructs).

Prior to use, all parts were sonicated with detergent, rinsed with deionized water, and treated with 70% isopropanol. Parts were air dried and assembled under aseptic conditions. The assembled mold undersides were coated with a thin layer of vacuum grease (Dow Corning, Midland, MI) to prevent the gel solution from spreading between the mold and the tissue-culture plastic of the 6-well plates in which they were seated. Fibrin adhesion to the bottom of the 6-well plates was minimized by soaking each well in 1 mL of 5.0% Pluronic F-127 (Sigma-Aldrich, St. Louis, MO) for 2 hours and air-drying before inserting the molds.

Fibrin Cruciform Preparation

Fibrin cruciforms were prepared in accord with established protocols [16,26]. Briefly, bovine fibrinogen (Sigma-Aldrich), bovine thrombin (Sigma-Aldrich), CaCl_2 , and nHDFs were combined to produce final construct concentrations of 6.6 mg/mL fibrinogen, 0.82 units/mL thrombin, 4.92 mM Ca^{2+} , and 0.5×10^6 cells/mL. Suspensions were incubated for 30 minutes at 37 °C in a humidified 95/5% air/ CO_2 incubator to allow gelation before culture medium was added. Culture medium consisted of high glucose DMEM supplemented with 10% FBS, 100 units/mL penicillin, 100 $\mu\text{g}/\text{mL}$ streptomycin, and 2.5 $\mu\text{g}/\text{mL}$ amphotericin-B, 2 $\mu\text{g}/\text{mL}$ insulin, 50 $\mu\text{g}/\text{mL}$ ascorbic acid (Sigma-Aldrich), and 1 ng/mL TGF- β (R&D Systems Inc., Minneapolis, MN). Medium was replaced three times a week for ten weeks.

Planar Equibiaxial Mechanical Testing and Polarimetric Imaging

In order to assess whether compositional changes led to differences in the cruciform mechanical response, samples were subjected to 5% equibiaxial stretch in the in-mold reference configuration. Prior to mechanical testing, samples were photographed, rinsed with phosphate buffered saline (PBS), and marked on the surface with Verhoeff's stain to enable strain analysis (Fig. 1C). Cruciforms were immersed in a 25 °C PBS bath and attached in-mold to the four 5N loads cells of an Instron planar biaxial testing unit. The molds were removed, and the cruciforms were subjected to a nominal 5% equibiaxial strain at a grip velocity of 0.3 mm/sec (1%/sec nominal strain rate). Because of the complex geometry and spatial heterogeneity of the samples, stress and strain are not meaningful in describing the mechanical response. Instead the force on each arm was recorded as a

function of grip displacement. The *stiffness* was calculated as the slope of the linear portion of the load-displacement curve. During testing, real-time fiber direction and strength of alignment was measured with polarimetric fiber alignment imaging [27]. Total testing time ranged from approximately 60 to 90 minutes for each sample.

Biochemical Analysis and Cell Number

Our analysis included both extensive measures (i.e., those that depend on sample size, such as total cell number) and intensive measures (e.g., cells per unit volume or dry weight). Intensive measures were used to facilitate comparisons between the two cruciform geometries, where were cast with the same concentration of cells and fibrin but differed in volume. Since it is possible that differences in fibrin degradation and/or cell proliferation occurred in the two cruciform geometries, which would complicate the use of dry weights for normalization needed to obtain intensive properties, extensive properties were also reported. After mechanical testing, the arms and center region of each construct were separated, and the dimensions and wet weights were recorded. Sample thickness in each region was calculated as the average of three measurements obtained with a low force probe [7]. Dry weight was determined after freezing (-20°C) and lyophilizing the samples. Cruciform surface area was calculated by counting the number of pixels contained within the cruciform boundary.

Mechanically tested samples were then subjected to biochemical analysis to measure total protein, elastin, and collagen content. Total protein and elastin were quantified with a modified ninhydrin assay [28], and collagen content was measured with the hydroxyproline assay [29]. Briefly, samples were hydrolyzed in 0.1 M NaOH at 98°C for 1 hour. The supernatant containing soluble protein was separated from the insoluble fraction containing elastin, which is highly cross-linked and survives the hot sodium hydroxide extraction as an insoluble pellet [30]. Both the insoluble pellet and the dried supernatant were hydrolyzed at 110°C in 6 N HCl for 24 hours and dried again. The hydroxyproline assay was conducted on the supernatant. The ninhydrin assay was conducted on the pellet and a fraction of the supernatant to measure total protein in the sample. Measured protein in the pellet was converted to elastin using purified alpha-elastin (Biocolor Life Science Assays, Carrickfergus, United Kingdom) as a standard. The standard was hydrolyzed and processed using identical methods to the pellet. The optical density of samples and corresponding standards were measured at 570 nm with a microplate reader (Bio-Tek Instruments, Inc., Winooski, VT). Collagen content was determined by converting measured hydroxyproline to collagen by assuming $7.46\ \mu\text{g}$ collagen per μg of hydroxyproline [31].

Cell number was measured on untested samples that were processed in the same manner. DNA content was measured with a modified Hoechst assay [32]. Samples were digested overnight at 56°C in digestion buffer (100 mM Tris, 50 mM EDTA, pH 7.4) containing 0.5 mg/mL proteinase K. 100 μL of sample digest was combined with 100 μL of Hoechst reagent (0.2 $\mu\text{g}/\text{mL}$ Hoeschst 33258, 2 M NaCl, 10 mM Tris, 1 mM EDTA, pH 7.4) in a clear-bottom, black 96-well plate. Fluorescence was measured at 360/460 nm (excitation/emission) in a microplate reader and converted to DNA content through the use of calf thymus DNA standards diluted in digestion buffer over the range 0 to 500 ng/mL. Cell number was determined by assuming 7.6 pg of DNA per cell [33]. To facilitate comparisons between the two geometries, we also calculated cell number per unit dry weight, to which we refer as the *cellularity*, an intensive measure of the density of cells in a specific construct.

Histology

Cruciforms were washed in phosphate buffered saline (PBS) and fixed in their molds with 4% paraformaldehyde at 4°C for three hours, rinsed with PBS and infiltrated with a 30%

sucrose, 5% DMSO (w/V) solution in PBS at 4 °C overnight, and immersed in a second infiltration solution containing 50% of the first infiltration solution and 50% OCT (Tissue-Tek, Torrance, CA) for 4 hours at room temperature. Each step was conducted on an orbital shaker. Finally, the samples were cut from the mold with a scalpel, embedded in 100% OCT, frozen, and sectioned into 9 μm thick enface sections. Alternating sections were stained with either Lillie's Trichrome stain or picrosirius red, which stains collagen and enhances its birefringence [34]. Images were acquired at x 10 with a color CCD camera. Picrosirius red stained sections were viewed between crossed linear polarizers.

Scanning Electron Microscopy

Two- and four-week samples from an identical parallel study were prepared for scanning electron microscopy (SEM). Prior to SEM imaging, constructs were fixed at room temperature on an orbital shaker for two hours with 2.5% gluteraldehyde in 0.1 M sucrose and 0.1 M sodium cacodylate (pH 7.2). After rinsing, constructs were stained with 1% osmium tetroxide for one hour. Samples were then subjected to serial dehydration with alcohol, freeze-fractured, critical point dried, and sputter coated with 1–2 nm of platinum. SEM images were acquired with a Hitachi S-900 Field-Emission SEM (Hitachi Ltd., Tokyo, Japan).

Average collagen fibril diameter was estimated from nine measurements made on different fibrils in an SEM image at a magnification of 150,000X (Figure 6). Measurements were made in Adobe Photoshop 9.0 with the measure tool by drawing a line perpendicular to the fibril axis. The pixels along the line were converted to nanometers by using the SEM scale bar.

Finite Element Model With Anisotropic Biphasic Theory (ABT)

The Anisotropic Biphasic Theory [11, 35] describes the development of fiber alignment in an initially homogeneous cell-populated gel as a result of cell tractions exerted on the matrix. Based on the geometry of the gel, the distribution of the cells in the gel, and the mechanical constraints on the gel, the model predicts how cell traction produces fiber alignment in the gel. A 3D adaptive finite element implementation of the ABT (described in [22, 35]) was used to simulate cell compaction of the cruciform geometries. To simulate the experiment, zero displacement was enforced at the ends of the arms, and all other surfaces were free surfaces. Model parameters were the same as those used in Jhun et al. [22]. The local fiber direction and strength of fiber alignment were calculated from the eigenvectors and eigenvalues of the fiber orientation tensor.

Statistical Analysis

Data are presented as mean values ± standard deviation. Statistical significance was evaluated in SPSS (SPSS, Chicago, IL). Significance ($p < 0.05$) was determined with a two-way analysis of variance (ANOVA) with time and geometry as factors. Bonferroni post hoc tests ($p < 0.05$) were applied when the outcome of an ANOVA indicated significance.

RESULTS

Changes in Construct Weight and Dimensions

The fibroblasts rapidly compacted fibrin gels of both cruciform geometries, decreasing the volume by approximately 85% – 90% over the duration of the experiment. During this process, the arms contracted both in-plane from the mold walls and through the thickness (Table 1). The arms were thickest near the glass rods and thinned as they approached the cruciform center, which contracted from 5 mm thick at formation to approximately 0.5 – 0.7 mm thick by week 5 (Table 1).

Extensive measurements (dry weight, wet weight, total protein) were significantly higher in the 1:1 cruciforms as expected because the 1:1 cruciforms by virtue of geometry were 28% greater in volume, and therefore contained more fibrin and cells at the start of the experiment than the 1:0.5 cruciforms. In both geometries, wet weight dropped significantly between weeks two and five, while dry weight and total protein did not change significantly over time (Table 1), an effect primarily due to compaction (i.e. gel syneresis).

Cell-exerted tractions were observed indirectly at week ten from the amount of retraction that occurred along each axis of a cruciform after it was released from the mold. Differences in axial retraction within a 1:1 cruciform were not found. The 1:0.5 cruciform generally displayed asymmetric axial retraction with the narrower 4 mm arms retracting more than the wider 8 mm. However, the response was highly variable and statistical differences in axial retraction within this geometry were not found. When data were averaged over all four arms, however, the 1:0.5 cruciforms exhibited more shortening than the 1:1 cruciforms after ten weeks of culture ($35\% \pm 3\%$ versus $28\% \pm 2\%$, respectively), illustrating differences in the mechanical environment between the two geometries.

Cell Number and Cellularity

Cell number increased significantly over time from an estimated 1.15 million cells to a measured 5.2 million cells in the 1:1 geometry, and from an estimated 0.9 million to a measured 4.6 million cells in the 1:0.5 geometry ($p < 0.001$) (Fig. 2A). When examined as a whole, cellularity (cell number normalized by dry weight) was not dependent on mold geometry and increased significantly from approximately 1.9×10^5 cells/mg at week two to 3.0×10^5 cells/mg at week five ($p < 0.05$) without significant change through week ten (Fig. 2B). Cell dry weight to total sample dry weight also did not depend on geometry, and at week ten reached $17.2\% \pm 0.8\%$ and $17.1\% \pm 2.0\%$ for 1:1 and 1:0.5 geometries, respectively. Taken as a fraction of total protein, cell protein only accounted for approximately 15% of the total protein at week ten. Significant regional differences in cellularity within each cruciform were only found at week five, with a higher cellularity in the arms compared to the center region for the 1:1 cruciform, and a higher cellularity in the narrower 4 mm arms than in other parts of 1:0.5 cruciform or any region of the 1:1 cruciform (Fig. 3B).

Elastin

During the remodeling process, the elastin produced by the cells accounted for less than 0.5% of the total protein in the cruciforms (Fig. 2C). Nevertheless, there was a five- to sixfold increase in the total amount of elastin produced in the constructs over the ten-week culture period, with more total elastin produced in the 1:0.5 geometry than in the 1:1 geometry ($p < 0.05$). Similar trends were observed when elastin was normalized by cell number (Table 2) or dry weight (Fig. 2D). Regional differences in normalized values within a cruciform were not significant (Fig. 3D).

Collagen

The total amount of collagen produced increased from approximately 100 μg at week two to 600 μg at week ten (Fig. 2E), with a significant increase in collagen at each time point ($p < 0.001$) but with no significant difference between the two geometries. This represents an increase from 1% of the total protein in the construct at week two to approximately 10% of the total protein by week ten. Significantly more collagen per construct dry weight was produced in the 1:0.5 geometry compared to the 1:1 geometry ($p < 0.05$) (Fig. 2F). Normalization by total protein (data not shown) and cell number (Table 2) produced similar trends. Regionally, significantly more collagen per dry weight was found in the 4 mm arms

of the 1:0.5 cruciform than elsewhere ($p < 0.05$) (Fig. 3F). The most collagen per cell was also produced in the narrower 4 mm arms (Table 2).

Histology and Scanning Electron Microscopy

For each time point and geometry, a cruciform was sectioned and stained with Lillie's trichrome stain in order to assess the spatial distribution of cells, collagen, and unremodeled fibrin (Fig. 4). After two weeks of remodeling, a band of collagen (bluish-green) approximately 70 – 100 μm thick and associated with a dense cell layer formed on the surface of the cruciform. The surface was characterized by a high collagen density (blue stain in the trichrome image and brighter picosirius red staining), high cell density, and low fibrin density (minimal red in the trichrome images). The interior, in contrast, showed a significant amount of undigested fibrin (more red in the trichrome image), lower cell density, and lower collagen density (dimmer picosirius red staining). The high fibrin density in the interior obscured the collagen staining in the trichrome images [7], which is revealed by the picosirius red staining.

Differences in the trichrome staining patterns amongst constructs were not apparent, in part because the large amount of undigested fibrin remaining in the constructs obscured the collagen beneath [7, 26]. To complement the trichrome images, alternating sample sections were stained with picosirius red so that collagen fiber organization throughout the constructs could be visualized (Fig. 4). These sections also showed a higher density of collagen on the surface, as well as a more diffuse network of interconnected collagen fibers spanning the interior (Fig. 4).

A more detailed view of the cruciform microstructure was provided by SEM images (Figs. 5 – 6). SEM images supported the histological findings of a dense cell layer at the surface of the cruciforms with fewer cells in the fibrin interior (Fig. 5). By week four, the emergence of collagen fibril bundles embedded in the interior fibrin matrix was more apparent (Fig. 6). Collagen fibers were distinguishable from the surrounding fibrin fibers by the characteristic appearance of parallel fibrils bundled together, attributes not found with fibrin fibers. Randomly sampled fibrils measured 33 ± 3 nm in diameter. Fibrous proteins were visible on the cell-coated construct surface, but these proteins did not possess the structure and organization that clearly identified the bundled collagen fibrils in the construct interior. As with the histological images, differences amongst samples were not readily apparent.

Mechanical Testing

The results of equibiaxial mechanical tests are given in Figure 7 and Table 3. The cruciform stiffness, that is the slope of the linear region of the force-displacement curve at the highest displacements, increased significantly ($p < 0.0001$) over the 10-wk experiment for both cruciform geometries, with the final stiffness roughly ten times higher than the initial stiffness. Because the samples were stiffer and the material around the mounting rod was thinner (due to cell-driven compaction and/or fibrinolysis) in the 10-wk samples, the load-displacement curve often exhibited yielding (the maximum in the load-displacement curve for the [horizontal] arms in Figure 7A) and/or failure at the grips (the premature end of the curves in Figure 7B). The horizontal:vertical stiffness ratio in the 1:0.5 sample decreased significantly between week 2 and week 5 and then held roughly steady through week 10.

Alignment Imaging

Alignment imaging via polarized light revealed that the 1:1 cruciforms possessed strong alignment in the arms along their axes and a center region that was close to isotropic (Fig. 8). The 1:0.5 cruciforms also possessed strong alignment in the arms, but the center region had moderate alignment in the direction of the wider arms.

DISCUSSION

Cross-shaped fibroblast-populated fibrin gels that differed in their initial fiber alignment pattern displayed total and regional differences in ECM synthesis. Even though the 1:1 cruciform was approximately 28% larger in volume, and thus contained more cells and fibrin at the start of the experiment than the 1:0.5 cruciform, both geometries produced the same total amount of collagen over the ten-week culture period. Moreover, the 1:0.5 cruciform contained significantly more total elastin, more elastin per sample dry weight, and more collagen per sample dry weight than the 1:1 cruciform. Regional differences in the synthesis rates were found as well, with more collagen per dry weight produced in the narrower 4 mm arms of the 1:0.5 cruciform than elsewhere in either cruciform. In addition to the biological variability inherent in cell experiments like these, some of the variability in the measured responses likely comes from small differences during gel casting and in the way the gels compact and produce the final state of fiber alignment. These differences can arise if the gel slips some and contracts inward along the glass rods during compaction, or it adheres to a portion of the mold during the initial compaction process. A few of these connections did form, and they were severed within the first few days after casting with a sterile probe.

Although differences in the regional material properties between the two cruciforms remain to be determined, increases in cruciform stiffness over time were correlated with production and incorporation of collagen and, to a lesser extent, elastin into the ECM. Earlier studies in our lab have also shown a strong correlation between increased mechanical properties and collagen content [36]. Similarly, small increases in elastin content were found then. We consider elastin deposition as important, and although the amounts here are likely too small to affect the construct mechanics, the differences were statistically significant and potentially important. Taken together, these results indicate that ECM synthesis and degradation progressed in a manner dependent on the cruciform geometry and the resulting mechanical environment for the cells.

Several studies have indicated that the state of the mechanical environment directs cell activity and modulates ECM synthesis and degradation [16–18,37–39]. Similar studies on fibroblast-populated fibrin disks with no in-plane fiber alignment found that application of cyclic equibiaxial stretch increased collagen content, stiffness, and strength in a dose-dependent manner (i.e. magnitude and duration) over static controls [40,41]. Even without externally applied loads, other studies have demonstrated the importance of internal tension in the matrix [20, 21, 42–44].

In this study, as the fibroblasts compacted the fibrin gels, fibrin fibers and cells in the initially homogeneous, isotropic constructs aligned to produce an anisotropic and heterogeneous material that was under non-uniform isometric tension. The cells exerted tractions on the fibers, pulling them inwards and creating tension between interconnected fibers that propagated throughout the construct [45]. The higher levels of retraction observed in 1:0.5 cruciforms upon release from the mold suggests that geometry-dependent differences in the state of tension existed between the two geometries. However, since in-mold forces were not measured, we also allow for the possibility that the state of tension was the same and that differences in retraction reflected a lower stiffness in the 1:0.5 cruciform. The most likely scenario is that variations in both tension and mechanical properties contributed to the disparity in retraction, especially since regional differences in tension within a cruciform are also implied from the alignment patterns obtained from polarized fiber alignment imaging (Fig. 8).

Even after 10 weeks of remodeling, the trichrome images revealed that a substantial amount of undigested fibrin remained in the interior of the cruciforms, which is typical in statically-cultured constructs using fibroblasts [7,36,46], but generally absent in cyclically stretched constructs [16]. The fibroblasts used in this study routinely demonstrate a low rate of fibrinolysis compared to other cell types, which is attributable to their low synthesis of plasminogen [36]. Trichrome stains non-collagenous proteins red, and when the measured sources that contribute to the amount of total protein in the sample are tallied – collagen, elastin, and cells represented 10%, 0.5% and 15% of the total protein, respectively – it becomes clear that a large fraction of the remaining 75% of the protein is likely undigested fibrin. Other fibroblast-synthesized ECM proteins were also undoubtedly present, as we have separately identified fibronectin with immunogold labeling [47] and proteoglycans with dimethylmethylene blue (unpublished data) under comparable conditions, but these proteins likely account for a small fraction of the total protein.

We recently found that fibrin degradation products led to more collagen deposition by vascular smooth muscle cells contained in fibrin hemispheres [48]. We have not explored this behavior with fibroblasts, but it is possible that regional differences in rate of fibrin degradation, which might be modulated by the mechanical environment as well, also contributed to remodeling responses observed here. Should such effects exist, they would likely be amplified with externally applied mechanical stimulation over long-term culture. In this study, samples were only subjected to mechanical testing once at the time of harvest. In previous work [46], preconditioned fibrin-based heart valve leaflets with a similar collagen content demonstrated a repeatable mechanical response, indicating that the time scale for the mechanical testing in this study was likely short relative to any tension-induced fibrinolysis.

Like the trichrome images, the picrosirius red images show a dense layer of collagen in the cell-dense surface layer, but these images also reveal that a less-dense interconnected network of collagen is present in the interior (Figure 4). We attribute the change in mechanical properties over time to an increase in collagen that interpenetrates the fibrin network. This finding is consistent with previous work in which increased ultimate tensile strength (UTS) and modulus were correlated with collagen content [36]. Other proteins may have some influence on the behavior as well, but the temporal correlation between increasing collagen levels and increasing construct stiffness suggests strongly that collagen is the major factor in the evolution of the construct mechanical properties.

A 3D finite element model of our anisotropic biphasic theory (ABT) [11,35] predicted fiber alignment patterns similar to the experimentally-measured patterns for the cruciforms used in this study (Fig. 8) as previously found for cruciforms made with collagen gel [22]. Most notably, the model successfully predicted the large central isotropic region in the 1:1 cruciform and the two islands of isotropy that were shifted from the cruciform center towards the vertical arms in the 1:0.5 case. These alignment patterns arise from the interplay between cell-compaction of the gel, the geometry of the gel, and the constraints applied to the gel. As the arm width aspect ratio increases, the center region increases in alignment along the axis of the wider arm. In the model, cells exert traction along the long axis of the elongated cell. Cell alignment follows fiber alignment, which develops from anisotropic strain in the fiber network resulting from mechanically-constrained cell-induced compaction of the fiber network. As a result, more total force develops, and hence more material compacts laterally along the wider axis than the narrower axis. However, some lateral compaction still occurs in the narrower axis, and islands of isotropy develop that are shifted from the center of the cruciform in accord with the difference in force/strain anisotropy between the axes.

The highest maximum principal stresses in the fiber network predicted by the model occurred in the regions in which the highest amounts of collagen per cell were found experimentally. For example, in the 1:1 cruciform, higher maximum principal stresses were predicted in the arms than in the center region, and more collagen per cell was found in the arms than in the center region. Similarly, for the 1:0.5 cruciform, higher maximum principal stresses were found in the narrower arms than elsewhere in either cruciform (except for the arm corners), and the most collagen per cell was found in the narrower arms.

We thus observe a correlation among three phenomena: *fiber alignment* (predicted and measured), *stress and strain* (predicted), and *collagen synthesis* (measured). The correlation between maximum principle stress and fiber alignment is consistent with many observations made both by us [11,35] and others [49,50]. Likewise, the correlation between tensile mechanical stress and remodeling has been made by numerous investigators using homogeneous, isotropic samples [40,51,52]. Separating stress effects from alignment effects is extremely difficult because of the tendency of cells in an aligned fiber network to align with the surrounding fibers via contact guidance [23]. Further complicating this separation is the fact that a fibrin gel exhibits viscoelastic fluid behavior, similar to a collagen gel, under compressive deformations relevant to cell induced gel compaction [53], and alignment has been shown to more directly correlate with principle strain (as assumed in the ABT), not stress, during compression of an unremodeled cell-populated collagen gel [54]. Thus, in these fibrin remodeling studies, the physical and biological mechanisms underlying the observed correlation likely evolve, first being related to fibrin alignment via the principal strains (and consequent cell alignment via contact guidance), and then being related to collagen alignment via the principal stresses and existing cell alignment.

It is imperative that one recognizes that the ABT does not predict ECM degradation or synthesis, and that it cannot describe the remodeling observed in fibrin cruciforms over many weeks of culture. Rather, the ABT describes the initial period of compaction with minimal fibrin degradation (corresponding roughly to the first few days of culture). Thus, it can be concluded that (1) the stress field and cellular mechanical environment change quantitatively but not qualitatively during subsequent culture, (2) the alignment state created during the initial fibrin compaction, which is preserved throughout the experiment, including the cell-deposited collagen, is providing the cues necessary to cause differences in the remodeling process, or (3) both of the previous two propositions, or (4) the agreement between the model predictions for short-time compaction and the experimentally-observed long-time remodeling is merely coincidence.

Possibility (1), that the inhomogeneity in the stress field is maintained throughout the remodeling process, is consistent with the well-known mediation of proliferation and synthetic activity by stress, so it must be considered. The regional variations in stress would be extremely difficult to measure in such a complex and heterogeneous material, so at present our only option is to observe that the calculated stress field matches the observed remodeling behavior, and that the effect of stress on remodeling is documented in simpler systems. The correlation does suggest that a theoretical model of remodeling should give strong consideration to a stress-dependent degradation/synthesis term [55–57]. Ruberti [58] has reported that collagen becomes more resistant to matrix-metalloproteinase (MMP) degradation with increased load. To our knowledge, a parallel experiment has not been done with fibrin. However, at least one study has shown increased fibrinolysis in free-floating fibrin gels populated with gingival fibroblasts as compared to anchored gels [59]. The free-floating gels had higher levels of tissue plasminogen activator in the medium compared to their anchored counterparts. This comparison represents two extremes, and it is unclear whether differences in fibrin tension in anchored constructs will cause fibrin degradation

through different mechanisms. Clearly, further investigation on this point is necessary and will greatly increase our understanding of remodeling under load.

Possibility (2), that alignment affects degradation and synthesis, is less well studied and is confounded by the common correlation between alignment and stress (e.g., in a uniaxial isometric system, [10, 59]). Aligned, homogeneous collagen and fibrin gels can be produced via fibrillogenesis in a strong magnetic field [60–62], but the resulting sample will drift toward isotropy in the absence of constraints to the subsequent cell-induced gel compaction [5], and any constraint would necessarily complicate the analysis by introducing stress. Thus, we again conclude that it may be that fiber alignment per se affects fibrin degradation and/or collagen synthesis, but that the current study was not conclusive in that regard. Given the body of evidence from simpler systems in support of the concepts of possibility (1), it merits further study, recognizing that other possibilities also exist.

For example, transport effects, which are notoriously difficult to uncouple from mechanical effects, may have played some role in the remodeling differences observed. Geometry-dependent differences in diffusion are possible, given that the gels compacted and remodeled in a heterogeneous fashion. Considering that sample thickness was the shortest dimension and approximately equal between geometries, diffusional differences seem unlikely. A related issue is that the cells in the 1:0.5 cruciforms received more nutrients per cell than those in the 1:1 cruciforms. This imbalance arose from the fact that both geometries were given equal volumes of medium (4 mL per well) even though the initial cell number was 28% greater for the 1:1 cruciform because of its larger volume different. While it would have been possible to proportion the medium volume so that on a per cell basis the nutrient concentrations were equal between the two geometries, the rapid growth of cells and other experimental considerations would have made this procedure difficult to maintain, let alone interpret, beyond the initial days of the experiment. For that reason, equal volumes of medium were used.

CONCLUSIONS

Cell-remodeled cross-shaped fibrin gels that differed in the aspect ratio of the arm widths (1:1 vs. 1:0.5) were studied to assess whether tension and alignment of the cells and fibers affected ECM deposition during fibrin remodeling. The remodeling response of the cruciforms was assessed at 2, 5, and 10 weeks of static culture with planar biaxial testing, polarimetric imaging, DNA and biochemical analyses, histological staining, and SEM imaging. Collagen increased in both cruciforms over 10 wks with no significant difference in the total amount between geometries even though the 1:0.5 geometry had approximately 28% fewer cells and starting material. The collagen per cell was increased in the narrow 4 mm arm of the 1:0.5 cruciform compared to any other region in either geometry, a result that corresponds with where the highest tensile stresses are predicted in ABT simulations of the cell-induced gel compaction and alignment. The simulations suggest that the regional mechanical stress environment that develops from reciprocal interactions between cell traction forces, cell contact guidance with aligned fibers, and the mechanical constraints on the gel, influences collagen deposition. Construct stiffness (assessed crudely) shows a temporal correlation with collagen deposition but a more sophisticated analysis will be required to understand geometry effects. Taken together, these results suggest that a high local mechanical stress produced via cell compaction and fiber alignment induces more collagen, and to a lesser extent, elastin synthesis, a conclusion consistent with the experience of our group [16,17] and others [18,39,40] that loading engineered tissues during incubation leads to better mechanical properties.

Acknowledgments

Support for this work was provided by the National Institutes of Health (R01 EB005813 and F32 EB007433). Parts of this work were carried out in the University of Minnesota I.T. Characterization Facility, which receives partial support from the National Science Foundation through the NNIN program. The authors thank Carry Valley, Naomi Ferguson, Sandy Johnson, Mike Evans, Chris Frethem, and Nat Dyment for technical support.

References

1. Butler DL, Goldstein SA, Guilak F. Functional Tissue Engineering: The Role of Biomechanics. *J Biomech Eng.* 2000; 122:570–575. [PubMed: 11192376]
2. Humphrey, JD. Cardiovascular Solid Mechanics: Cells, Tissues, and Organs. Springer; New York: 2002.
3. Fratzl, P. Collagen: Structure and Mechanics. Springer; New York: 2008.
4. Harris AK, Stopak D, Wild P. Fibroblast Traction as a Mechanism for Collagen Morphogenesis. *Nature.* 1981; 290:249–251. [PubMed: 7207616]
5. Barocas VH, Girton TS, Tranquillo RT. Engineered Alignment in Media Equivalents: Magnetic Prealignment and Mandrel Compaction. *J Biomech Eng.* 1998; 120:660–666. [PubMed: 10412446]
6. Neidert MR, Tranquillo RT. Tissue-Engineered Valves With Commissural Alignment. *Tissue Eng.* 2006; 12:891–903. [PubMed: 16674301]
7. Robinson PS, Johnson SL, Evans MC, Barocas VH, Tranquillo RT. Functional Tissue-Engineered Valves from Cell-Remodeled Fibrin with Commissural Alignment of Cell-Produced Collagen. *Tissue Eng Part A.* 2008; 14:83–95. [PubMed: 18333807]
8. Grassl ED, Oegema TR, Tranquillo RT. A Fibrin-Based Arterial Media Equivalent. *J Biomed Mater Res.* 2003; 66:550–561.
9. Shi Y, Rittman L, Vesely I. Novel Geometries for Tissue-Engineered Tendonous Collagen Constructs. *Tissue Eng.* 2006; 12:2601–2609. [PubMed: 16995793]
10. Juncosa-Melvin N, Boivin GP, Galloway MT, Gooch C, West JR, Sklenka AM, Butler DL. Effects of Cell-to-Collagen Ratio in Mesenchymal Stem Cell-Seeded Implants on Tendon Repair and Biomechanics and Histology. *Tissue Eng.* 2005; 11:448–457. [PubMed: 15869423]
11. Barocas VH, Tranquillo RT. An Anisotropic Biphasic Theory of Tissue-Equivalent Mechanics: The Interplay Among Cell Traction, Fibrillar Network Deformation, Fibril Alignment, and Cell Contact Guidance. *J Biomech Eng.* 1997; 119:137–146. [PubMed: 9168388]
12. Long JL, Tranquillo RT. Elastic Fiber Production in Cardiovascular Tissue-Equivalents. *Matrix Biol.* 2003; 22:339–350. [PubMed: 12935818]
13. Ross JJ, Tranquillo RT. ECM Gene Expression Correlates With In Vitro Growth and Development in Fibrin Gel Remodeled Remodeled By Neonatal Smooth Muscle Cells. *Matrix Biol.* 2003; 22:477–490. [PubMed: 14667840]
14. Yao L, Swartz DD, Gugino SF, Russell JA, Andreadis ST. Fibrin-Based Tissue-Engineered Blood Vessels: Differential Effects of Biomaterial and Culture Parameters on Mechanical Strength and Vascular Reactivity. *Tissue Eng.* 2005; 11:991–1003. [PubMed: 16144435]
15. Grouf JL, Thom AM, Balestrini JL, Bush KA, Billiar KL. Differential Effects of EGF and TGF- β 1 on Fibroblast Activity in Fibrin-Based Tissue Equivalents. *Tissue Eng.* 13:799–807. [PubMed: 17346099]
16. Syedain ZH, Weinberg JS, Tranquillo RT. Cyclic Distension of Fibrin-Based Tissue Constructs: Evidence of Adaptation During Growth of Engineered Connective Tissue. *PNAS.* 2008; 105:6537–6542. [PubMed: 18436647]
17. Isenberg BC, Tranquillo RT. Long-term Cyclic Distension Enhances the Mechanical Properties of Collagen-Based Media Equivalents. *Ann Biomed Eng.* 2003; 31:937–949. [PubMed: 12918909]
18. Stegemann JP, Nerem RM. Phenotype Modulation in Vascular Tissue Using Biochemical and Mechanical Stimulation. *Ann Biomed Eng.* 2003; 31:15–159.
19. Sander, EA.; Barocas, VH. Biomimetic Collagen Tissues: Collagenous Tissue Engineering and Other Applications. In: Fratzl, P., editor. *Collagen: Structure and Mechanics.* Springer; New York: 2008.

20. Grinnell F, Zhu M, Carlson MA, Abrams JM. Release of Mechanical Tension Triggers Apoptosis of Human Fibroblasts in a Model of Regressing Granulation Tissue. *Exp Cell Res.* 1999; 248:608–619. [PubMed: 10222153]
21. Nakagawa S, Pawelek P, Grinnell F. Extracellular Matrix Organization Modulates Fibroblast Growth and Growth Factor Responsiveness. *Exp Cell Res.* 1989; 182:572–582. [PubMed: 2721593]
22. Jhun C, Evans MC, Barocas VH, Tranquillo RT. Planar Biaxial Mechanical Behavior of Bioartificial Tissues Possessing Prescribed Fiber Alignment. *J Biomech Eng.* 2008; 131:081006. [PubMed: 19604018]
23. Tranquillo RT. Self-organization of Tissue Equivalents: The Nature and Role of Contact Guidance. *Biochem Soc Symp.* 1999; 65:27–42. [PubMed: 10320931]
24. Sander EA, Stylianopoulos T, Tranquillo RT, Barocas VH. Image-Based Biomechanics of Collagen-Based Tissue Equivalents: Multiscale Models Compared to Fiber Alignment Predicted by Polarimetric Imaging. *IEEE Eng Med Biol Mag.* 2008; 28(3):10–18. [PubMed: 19457729]
25. Sander EA, Stylianopoulos T, Tranquillo RT, Barocas VH. Image-Based Multiscale Modeling Predicts Tissue-Level and Network-Level Fiber Reorganization in Stretched Cell-Compacted Collagen Gels. *PNAS.* 2009; 106:17675–17680. [PubMed: 19805118]
26. Williams C, Johnson SL, Robinson PS, Tranquillo RT. Cell Sourcing and Culture Conditions for Fibrin-Based Valve Constructs. *Tissue Eng.* 12:1489–1502. [PubMed: 16846346]
27. Tower TT, Neidert MR, Tranquillo RT. Fiber Alignment Imaging During Mechanical Testing of Soft Tissues. *Ann Biomed Eng.* 2002; 30:1221–1233. [PubMed: 12540198]
28. Starcher B. A Ninhydrin-based Assay to Quantitate the Total Protein Content of Tissue Samples. *Anal Biochem.* 2001; 292:125–129. [PubMed: 11319826]
29. Stegemann H, Stalder K. Determination of hydroxyproline. *Clin Chim Acta.* 1967; 18:267–273. [PubMed: 4864804]
30. Mecham RP. Methods in Elastic Tissue Biology, Elastin Isolation and Purification. *Methods.* 45:32–41. [PubMed: 18442703]
31. Dombi GW, Haut RC, Sullivan WG. Correlation of High-Speed Tensile Strength with Collagen Content in Control and Lathyrin Rat Skin. *J Surg Res.* 1993; 54:195–229.
32. Kim YJ, Sah RL, Doong JY, Grodzinsky AJ. Fluorometric Assay of DNA in Cartilage Explants Using Hoechst 33258. *Anal Biochem.* 1998; 174:168–176. [PubMed: 2464289]
33. Kim BS, Mooney DJ. Engineered Smooth Muscle Tissue With A Predefined Structure. *J Biomed Mater Res.* 1998; 41:322–332. [PubMed: 9638538]
34. Junqueira LCU, Bignolas G, Brentani RR. Picrosirius staining plus polarization microscopy, a specific method for collagen detection in tissue sections. *Histochemical Journal.* 1979; 11:447–455. [PubMed: 91593]
35. Oshumi TK, Flaherty JE, Evans MC, Barocas VH. Three-Dimensional Simulation of Anisotropic Cell-Driven Compaction. *Biomech Model Mechanobiol.* 2008; 7:53–62. [PubMed: 17354006]
36. Neidert MR, Lee ES, Oegema TR, Tranquillo RT. Enhanced Fibrin Remodeling in Vitro with TGF-beta1, insulin and plasmin for improved tissue-equivalents. *Biomaterials.* 2002; 23:3717–31. [PubMed: 12109697]
37. Prajapati RT, Chavally-Mis B, Herbage D, Eastwood M, Brown RA. Mechanical Loading Regulates Protease Production by Fibroblasts in Three-Dimensional Collagen Substrates. *Wound Rep Reg.* 2000; 8:226–237.
38. Seliktar D, Nerem RM, Galis ZS. Mechanical Strain-Stimulated Remodeling of Tissue-Engineered Blood Vessel Constructs. *Tissue Eng.* 2003; 9:657–666. [PubMed: 13678444]
39. Boerboom RA, Rubbens MP, Driessen NJ, Bouten CV, Baaijens FP. Effect of Strain Magnitude on the Tissue Properties of Engineered Cardiovascular Constructs. *Ann Biomed Eng.* 2008; 36:244–53. [PubMed: 18066665]
40. Balestrini JL, Billiar KL. Equibiaxial Cyclic Stretch Stimulates Fibroblasts to Rapidly Remodel Fibrin. *J Biomech.* 2006; 39:2983–90. [PubMed: 16386746]
41. Balestrini JL, Billiar KL. Magnitude and Duration of Stretch Modulate Fibroblast Remodeling. *J Biomech Eng.* 2009; 131:051005. [PubMed: 19388775]

42. Mochitate K, Pawelek P, Grinnell F. Stress Relaxation of Contracted Collagen Gels: Disruption of Actin Filament Bundles, Release of Cell Surface Fibronectin, and Down-Regulation of DNA and Protein Synthesis. *Exp Cell Res.* 1991; 193:198–207. [PubMed: 1995294]
43. Arora PD, Narani N, McCulloch CAG. The Compliance of Collagen Gels Regulates Transforming Growth Factor- β Induction of α -Smooth Muscle Actin in Fibroblasts. *American Journal of Pathology.* 1999; 154:871–882. [PubMed: 10079265]
44. Trachslin J, Koch M, Chiquet M. Rapid and Reversible Regulation of Collagen XII Expression by Changes in Tensile Stress. *Exp Cell Res.* 1999; 247:320–328. [PubMed: 10066359]
45. Grinnell F. Fibroblast-Collagen-Matrix Contraction: Growth-Factor Signaling and Mechanical Loading. *Trends Cell Biol.* 2000; 10:362–365. [PubMed: 10932093]
46. Ahmann KA, Weinbaum JS, Johnson SL, Tranquillo RT. Fibrin Degradation Enhances Vascular Smooth Muscle Cell Proliferation and Matrix Deposition in Fibrin-Based Tissue Constructs Fabricated In Vitro. *Tissue Eng Part A.* 2010 -Not available-, ahead of print. 10.1089/ten.tea.2009.0708
47. Sander EA, Johnson SL, Barocas VH, Tranquillo RT. Matrix Remodeling in Fibroblast –Seeded Fibrin Gels. *Matrix Biology.* 2008; 27:28.
48. Robinson PS, Tranquillo RT. Planar Biaxial Behavior of Native and Tissue-Engineered Heart Valve Leaflets. *Tissue Eng Part A.* 2009; 15:2763–72. [PubMed: 19368523]
49. Eastwood M, Mudera VC, McGrouther DA, Brown RA. Effects of Precise Mechanical Loading on Fibroblast Populated Collagen Lattices: Morphological Changes. *Cell Motility and the Cytoskeleton.* 1998; 40:13–21. [PubMed: 9605968]
50. Hariton I, de Botton G, Gasser TC, Holzapfel GA. Stress-Driven Collagen Fiber Remodeling in Arterial Walls. *Biomechanics and Modeling in Mechanobiology.* 2007; 6:163–175. [PubMed: 16912884]
51. Knezevic V, Sim AJ, Borg TK, Holmes JW. Isotonic Biaxial Loading of Fibroblast-Populated Collagen Gels: A Versatile, Low-Cost System for the Study of Mechanobiology. *Biomechan Model Mechanobiol.* 2002; 1:59–67.
52. Lee EJ, Holmes JW, Costa KD. Remodeling of Engineered Tissue Anisotropy in Response to Altered Loading Conditions. *Ann Biomed Eng.* 36:1322–1334. [PubMed: 18470621]
53. Knapp DM, Barocas VH, Moon AG, Yoo K, Petzold LR, Tranquillo RT. Rheology of Reconstituted Type I Collagen Gel in Confined Compression. *J Rheol.* 1997; 41:971–993.
54. Girton TS, Barocas VH, Tranquillo RT. Confined Compression of a Tissue-Equivalent: Collagen Fibril and Cell Alignment in Response to Anisotropic Strain. *J Biomech Eng.* 2002; 124:568–575. [PubMed: 12405600]
55. Gleason RL, Humphrey JD. Effects of a Sustained Extension on Arterial Growth and Remodeling: A Theoretical Study. *J Biomech.* 2005; 38:1255–1261. [PubMed: 15863110]
56. Driessen NJB, Wilson W, Bouten CVC, Baaijens FPT. A Computational Model for Collagen Fibre Remodelling in the Arterial Wall. *J Theo Biol.* 2004; 226:53–64.
57. Kuhl E, Holzapfel GA. A Continuum Model for Remodeling in Living Structures. *J Mat Sci.* 2007; 42:8811–8823.
58. Ruberti JW, Hallab NJ. Strain-controlled Enzymatic Cleavage of Collagen in Loaded Matrix. *Biochemical and Biophysical Research.* 2005; 336:483–489.
59. Lorimier S, Bouthors S, Droulle C, Maquin DL, Maquart F, Gillery P, Emonard H, Hornebeck W. The Rate of Fibrinolysis is Increased by Free Retraction of Human Gingival Fibroblast Populated Fibrin Lattices. *Int J Biochem Cell Biol.* 1997; 29:181–189. [PubMed: 9076953]
60. Shi Y, Vesely I. Characterization of Statically Loaded Tissue-Engineered Mitral Valve Chordae Tendineae. *J Biomed Mater Res.* 2004; 69A:26–39.
61. Freyssinet JM, Torber J, Hudry-Clergeon G. Fibrinogen and Fibrin in Strong Magnetic Fields. Complementary Results and Discussion. *Biochimie.* 1984; 66:81–85. [PubMed: 6733156]
62. Dubey N, Letourneau PC, Tranquillo RT. Guided Neurite Elongation and Schwann Cell Invasion Into Magnetically Aligned Collagen in Simulated Peripheral Nerve Regeneration. *Experimental Neurology.* 1999; 158:338–350. [PubMed: 10415141]

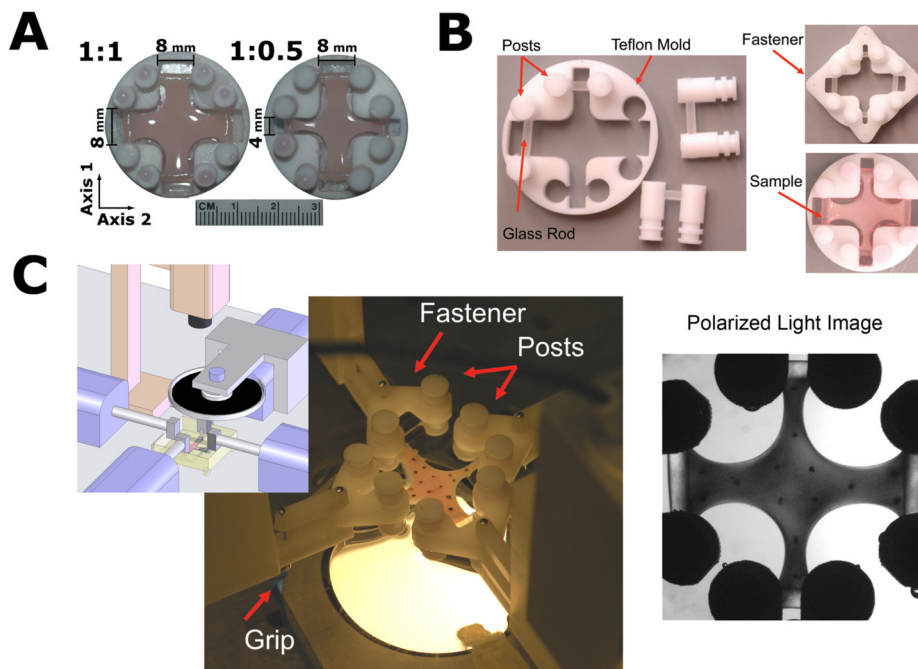


Figure 1.

(A) Cruciform geometries. The cruciforms differ in axis channel width, which produces different fiber alignment patterns in the cruciform center. (B) Redesigned molds allow for casting with the fixtures necessary for mechanical testing already in place. Glass rods span each channel and secure the fibrin gel as it compacts. To facilitate mechanical testing in the in-mold reference configuration, fasteners are attached to the posts, which connect to the mechanical testing system. (C) Inset shows a schematic of the imaging and mechanical testing system. Once the sample is secured in the grips, the mold slides off, and testing begins. Polarized light images are acquired during testing.

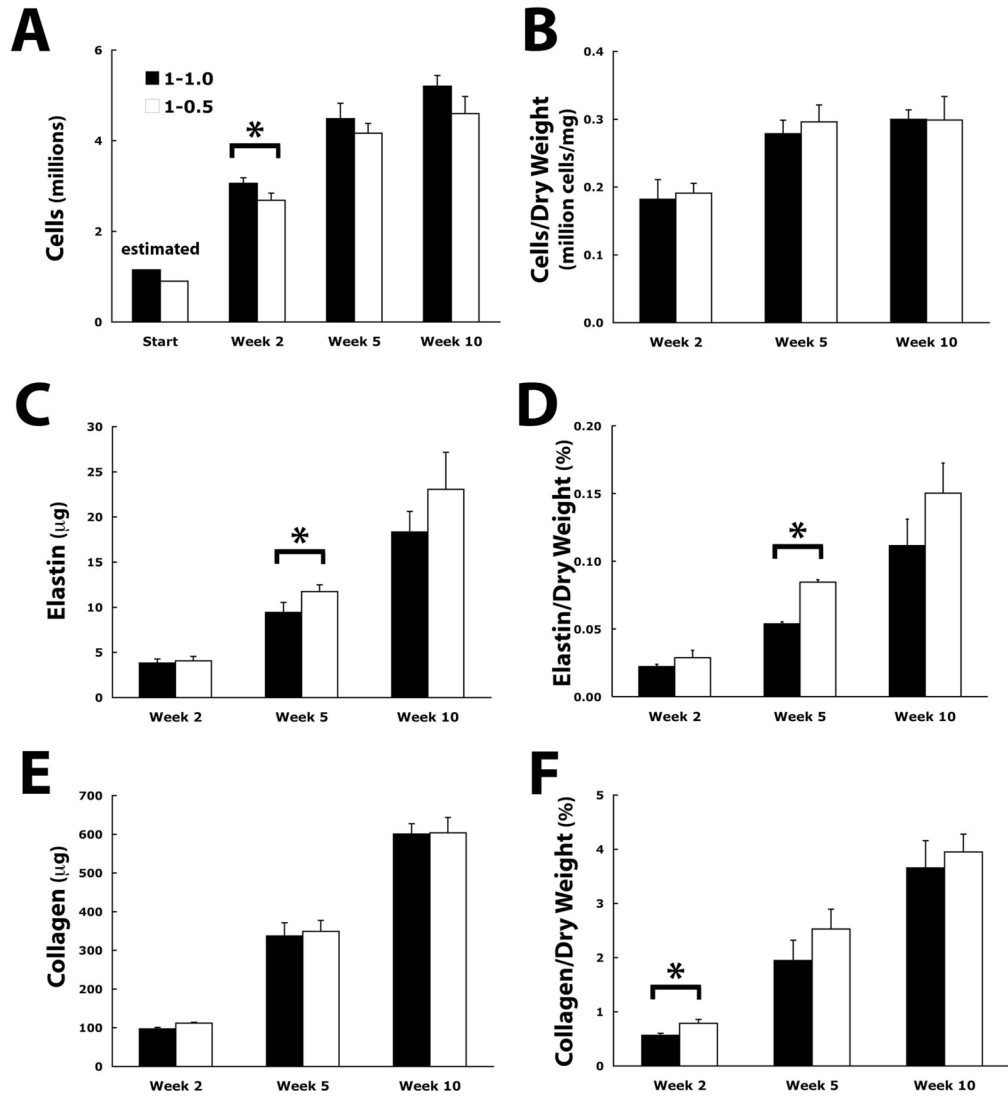


Figure 2. (A, C, E) Differences in whole cruciform cell number, elastin, and collagen between the 1:1 and 1:0.5 cruciform over the ten-week culture period. (B, D, F) Data normalized by sample cruciform dry weight. All data showed a significant difference between time points except for (B) cells/dry weight week 5 and week 10. Measurements with a significant difference ($p < 0.05$) between 1:1 and 1:0.5 cruciforms are marked with an asterisk

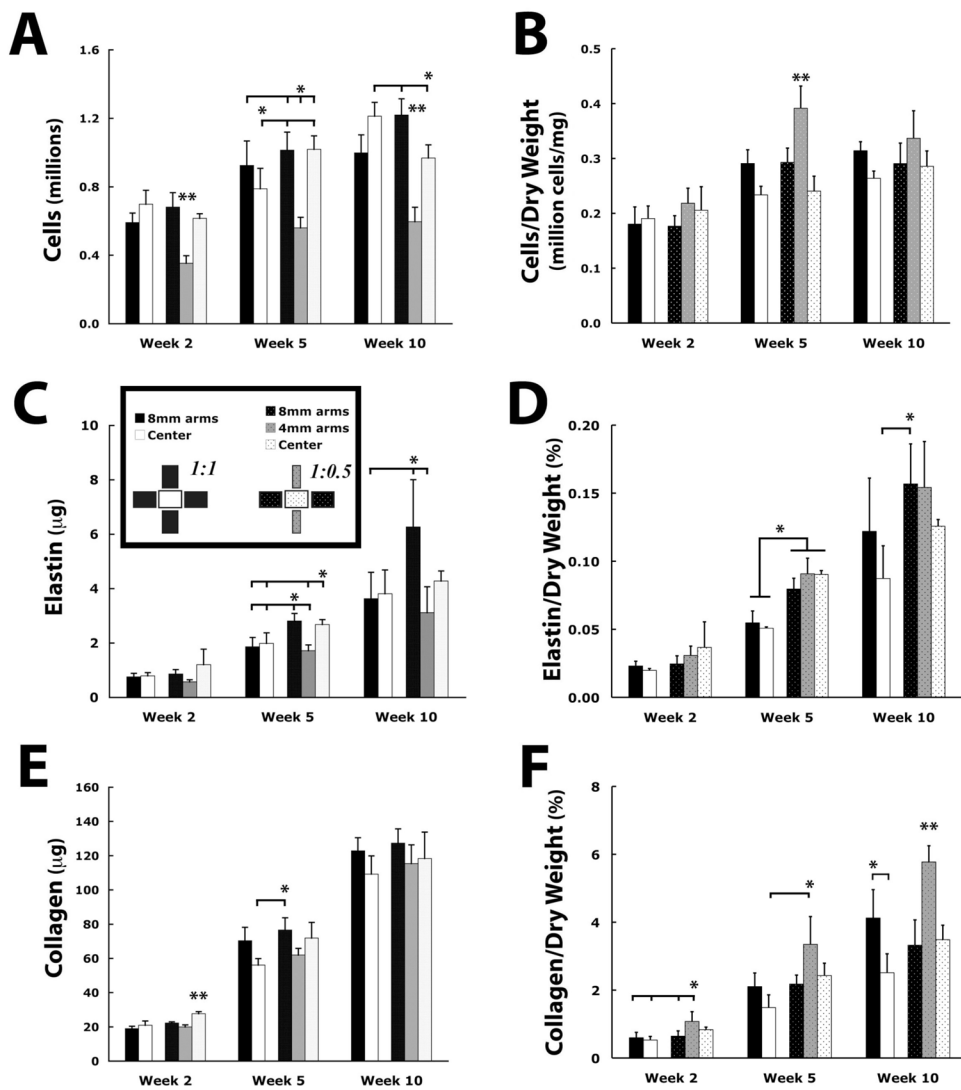


Figure 3. (A, C, E) Regional differences in cell number, elastin, and collagen. (B, D, F) Data normalized by regional dry weight. *: ($p < 0.05$) with indicated regions, **: ($p < 0.05$) with all regions.

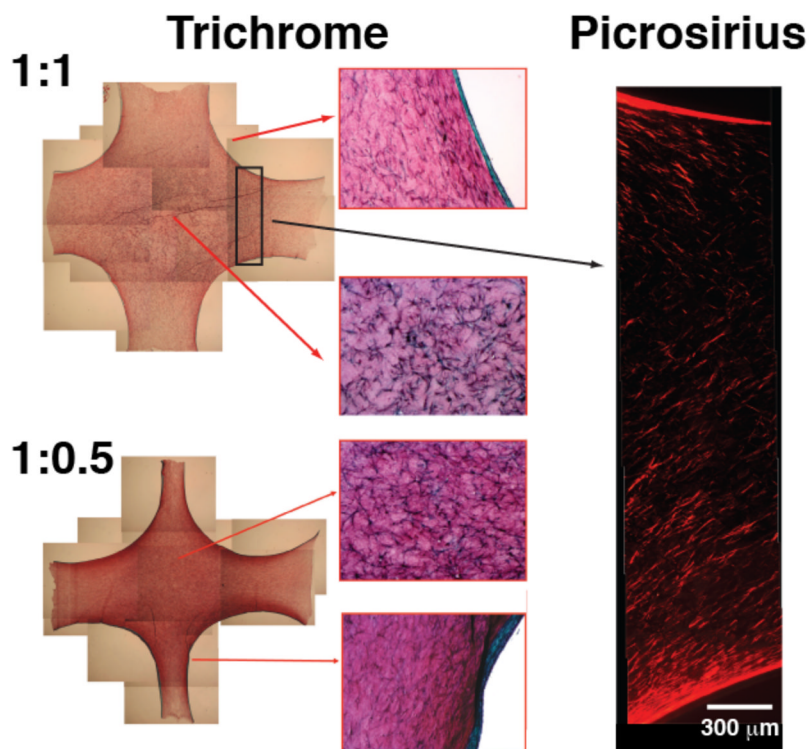


Figure 4. Lillie's trichrome staining after ten weeks. Sections are through the mid-plane for both geometries. Trichrome stains collagen bluish-green and non-collagenous proteins red. A thick band of collagen associated with a layer of cells at the construct surface encapsulated the cruciforms. Both cruciform interiors were predominantly red, indicating that a large amount of residual fibrin remained. In the interior, cells were more spread out and lower in density than at the surface. Collagen was also associated with these cells as indicated by pericellular blue staining. A representative picrosirius red stained section from the midplane (through the thickness) also confirms a dense collagen layer on the periphery and less dense interior. It shows a slice of the arm as it widens towards the center region.

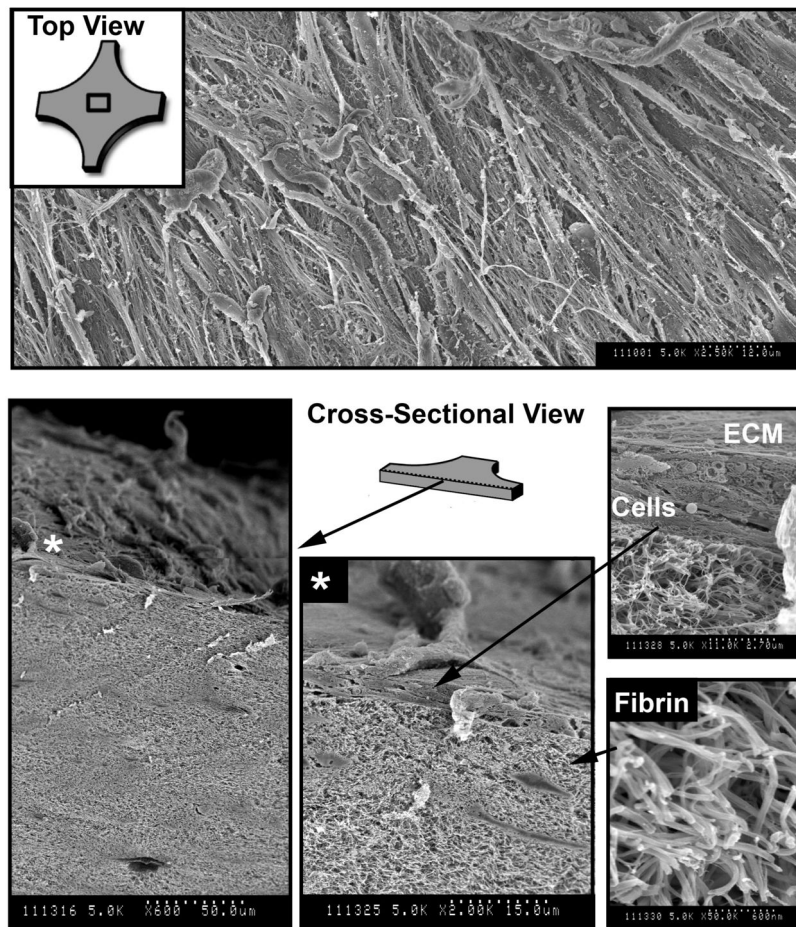


Figure 5. Representative SEM images of the cruciforms after two weeks. (Top) A thin layer of cells formed on the cruciform surface. (Bottom) A cross-sectional view shows the cell layer on top of largely undigested but compacted fibrin matrix. A magnified view (asterisk shows location) clearly shows a raised cell with processes above a layer comprised of at least two cells. Above the cell layer are a variety of unidentified fibrillar ECM components. Based on trichrome staining, many of these fibers are expected to be collagen.

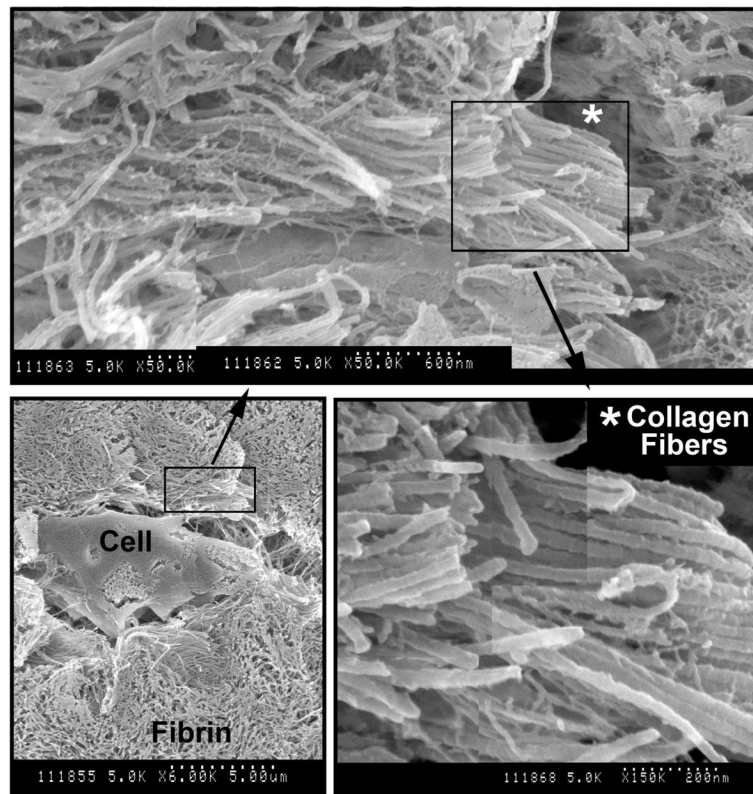


Figure 6. Representative SEM images of the construct interior after four weeks. Depicted in the bottom left image is a cell embedded in the fibrin matrix. By week four, the emergence of collagen fibril bundles embedded in the fibrin matrix becomes more apparent. In the top image, collagen parallel fibril bundles can be identified from the surrounding fibrin by both the parallel bundling and the characteristic banding pattern on the fibrils. The asterisk shows the location of the magnified region on the bottom right. Collagen fibrils in the interior were always identified near cellular material.

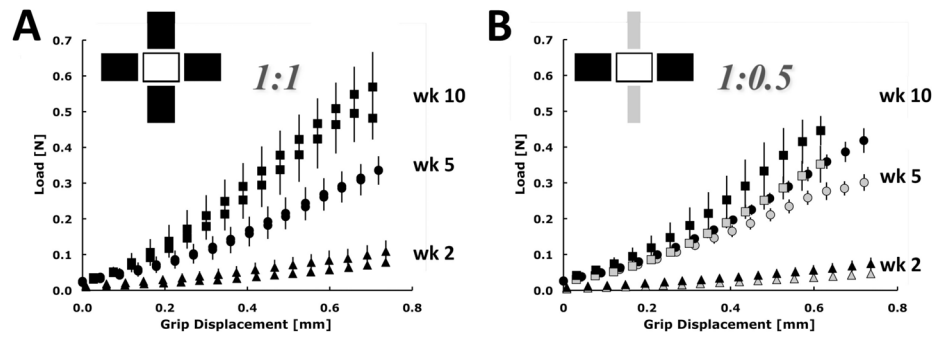


Figure 7.

Average axis load vs. grip displacement for the 1:1 cruciform (A) and 1:0.5 cruciform (B). The data are plotted as the mean and standard deviation of the three samples tested at each time point (wk2 – triangle, wk5 – circle, wk10 – square) and color coded with the cruciform representations shown above to indicate which arm geometry is represented in the plots. For the 1:0.5 geometry, the wider arm is depicted in black and the narrower arm in gray. Stiffness assessed from the linear region of the curves increased significantly with time ($p < 0.0001$).

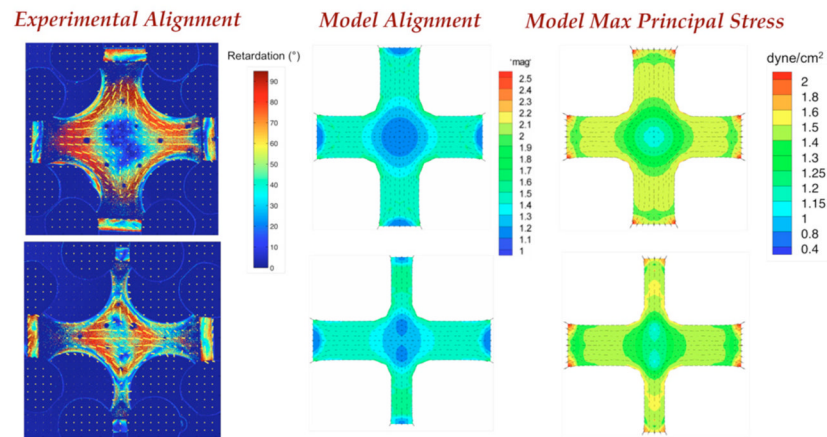


Figure 8. Fiber Alignment and Stress

(Left) Polarimetric fiber alignment images show the local direction and strength of fiber alignment. In the 1:1 geometry (top), the horizontal and vertical arms are highly aligned and the center region is close to isotropic. In the 1:0.5 geometry (bottom) the center has some alignment in the center with two regions of isotropy shifted towards the vertical arms.

(Middle) Anisotropic biphasic theory (ABT) simulations of cell compaction capture the alignment patterns observed experimentally. **(Right)** ABT simulations predict a heterogeneous mechanical environment that differs between the two geometries. Note the high regions of stress in the narrow arms of the 1:0.5 cruciform.

Table 1

Construct Weight, Total Protein, and Dimensions Over Time

Geometry	Week	Wet Weight (mg)	Dry Weight (mg)	Total Protein (mg)	Thickness 8mm arms (μm)	Thickness 4mm arms (μm)	Thickness Center (μm)	Surface Area (mm^2)
1:1	2	203 \pm 39	17.2 \pm 2.1	9.08 \pm 0.78	911 \pm 131	-	926 \pm 121	329 \pm 3
	5	166 \pm 23	16.8 \pm 1.6	8.28 \pm 0.59	798 \pm 108	-	491 \pm 61	314 \pm 11
	10	161 \pm 17	17.0 \pm 1.4	7.85 \pm 0.88	774 \pm 167	-	514 \pm 50	298 \pm 6
1:0.5	2	165 \pm 9	14.2 \pm 1.2	6.94 \pm 0.37	1044 \pm 87	888 \pm 164	968 \pm 43	229 \pm 11
	5	136 \pm 19	14.0 \pm 0.9	6.11 \pm 0.63	902 \pm 197	876 \pm 111	666 \pm 125	216 \pm 2
	10	136 \pm 5	15.4 \pm 1.0	6.73 \pm 0.18	996 \pm 204	884 \pm 186	688 \pm 95	210 \pm 5

* Initial sample thickness was 5 mm at casting. Data are mean \pm standard deviation

Table 2

Cell Synthesized Elastin and Collagen Normalized by Cell Number

Geometry	Week	Elastin (pg/cell)						Collagen (pg/cell)					
		Whole		Regional		Whole		Regional		Whole		Regional	
		8mm arm	4mm arm	8mm arm	4mm arm	Center	4mm arm	Center	8mm arm	4mm arm	Center	4mm arm	Center
1:1	2	1.3 ± 0.2	1.3 ± 0.3	-	-	1.1 ± 0.2	31.7 ± 2.6	32.2 ± 6.2	-	-	30.0 ± 5.0	-	-
	5	2.1 ± 0.2	2.0 ± 0.5	-	-	2.5 ± 0.6	75.2 ± 9.7	76.1 ± 14.2	-	-	71.2 ± 11.7	-	-
	10	3.5 ± 0.3	3.6 ± 1.1	-	-	3.1 ± 0.8	115.4 ± 3.0	123.1 ± 19.2	-	-	90.0 ± 10.6	-	-
1:0.5	2	1.5 ± 0.2	1.3 ± 0.3	1.6 ± 0.3	2.0 ± 0.9	41.8 ± 2.5	83.8 ± 4.2	32.7 ± 6.0	56.4 ± 8.3	45.0 ± 2.7	110.7 ± 15.6	70.5 ± 10.5	122.3 ± 18.6
	5	2.8 ± 0.3	2.8 ± 0.4	3.1 ± 0.5	2.6 ± 0.3	83.8 ± 4.2	131.3 ± 4.2	75.5 ± 10.8	193.8 ± 35.4	104.4 ± 10.3	193.8 ± 35.4	122.3 ± 18.6	122.3 ± 18.6
	10	5.0 ± 0.7	5.1 ± 1.5	5.2 ± 1.8	4.4 ± 0.5	131.3 ± 4.2	131.3 ± 4.2	104.4 ± 10.3	193.8 ± 35.4	122.3 ± 18.6	193.8 ± 35.4	122.3 ± 18.6	122.3 ± 18.6

Data are mean ± standard deviation

Table 3

Stiffness Along Each Cruciform Axis Over Time

Geometry	Axis	Stiffness (N/mm)		
		Week 2	Week 5	Week 10
1:1	Horizontal (8 mm)	0.12 ± 0.04	0.56 ± 0.02	0.95 ± 0.11
	Vertical (8 mm)	0.09 ± 0.03	0.54 ± 0.01	0.92 ± 0.08
1:0.5	Horizontal (8 mm)	0.1 ± 0.02	0.65 ± 0.07	0.94 ± 0.11
	Vertical (4 mm)	0.06 ± 0.01	0.47 ± 0.03	0.72 ± 0.13

Data are mean ± standard deviation